



Material and manufacturing cost considerations for thermoelectrics



Saniya LeBlanc^{a,b,e,*}, Shannon K. Yee^{c,d,1}, Matthew L. Scullin^e, Chris Dames^d,
Kenneth E. Goodson^b

^a The George Washington University, Department of Mechanical & Aerospace Engineering, 801 22nd St. NW, Suite 739, Washington, DC 20052, USA

^b Stanford University, Department of Mechanical Engineering, Building 530, 440 Escondido Mall, Stanford, CA 94305, USA

^c Georgia Institute of Technology, George W. Woodruff School of Mechanical Engineering, Atlanta, GA 30332, USA

^d University of California – Berkeley, Department of Mechanical Engineering, 6141 Etcheverry Hall, Berkeley, CA 94720, USA

^e Alphabet Energy, Inc., 26225 Eden Landing Road, Suite D, Hayward, CA 94545, USA

ARTICLE INFO

Article history:

Received 6 June 2013

Received in revised form

18 November 2013

Accepted 18 December 2013

Keywords:

Thermoelectric cost

Thermoelectric \$/W

Thermoelectric manufacturing

ABSTRACT

Interest in thermoelectrics for waste-heat recovery and localized cooling has flourished in recent years, but questions about cost and scalability remain unanswered. This work investigates the fabrication costs and coupled thermal and electrical transport factors that govern device efficiency and commercial feasibility of the most promising thermoelectric materials. For 30 bulk and thin film thermoelectric materials, we quantify the tradeoff between efficiency and cost considering electrical and thermal transport at the system level, raw material prices, system component costs, and estimated manufacturing costs. This work neglects the cost of heat, as appropriate for most waste-heat recovery applications, and applies a power generation cost metric in \$/W and a cooling operating cost metric in \$/kWh. The results indicate material costs are too high for typical thermoelectric power generation applications at mean temperatures below 135 °C. Above 275 °C, many bulk thermoelectric materials can achieve costs below \$1/W. The major barrier to economical thermoelectric power generation at these higher temperatures results from system costs for heat exchangers and ceramic plates. For cooling applications, we find that several thermoelectric materials can be cost competitive and commercially promising.

© 2014 Elsevier Ltd. All rights reserved.

Contents

| | |
|--|----|
| 1. Introduction | 2 |
| 2. Methods | 4 |
| 2.1. Device physics | 5 |
| 2.1.1. Power generation | 5 |
| 2.1.2. Levelized cost of energy considerations | 7 |
| 2.1.3. Thermoelectric cooling | 7 |
| 2.2. Cost considerations | 7 |
| 2.3. Methods summary | 8 |
| 3. Results and discussion | 9 |
| 3.1. Material and module manufacturing costs | 9 |
| 3.2. Thermoelectric power generation | 10 |
| 3.3. Thermoelectric cooling | 11 |
| 3.4. Thermoelectric device targets summary | 13 |
| 4. Conclusion | 13 |
| Acknowledgments | 13 |
| Appendix A. Supporting information | 13 |
| References | 13 |

* Corresponding author at: The George Washington University, Department of Mechanical & Aerospace Engineering, 801 22nd St. NW, Suite 739, Washington, DC 20052, USA. Tel.: +1 202 994 8436; fax: +1 202 994 0238.

E-mail addresses: sleblanc@gwu.edu (S. LeBlanc), shannon.yee@me.gatech.edu (S.K. Yee), matt@alphabetenergy.com (M.L. Scullin).

¹ Indicates joint first authorship.

Nomenclature

| | | | |
|-----------|--|------------|--|
| A | total plate area (m^2) | LCOE | levelized cost of electricity ($\$/\text{kWh}$) |
| $A_{c,i}$ | thermoelectric leg i cross sectional area (m^2) | m | ratio of load resistance to device resistance |
| A_{TE} | total thermoelectric material cross sectional area (m^2) | max | subscript designating maximum value |
| C | total capital cost ($\$$) | n | subscript designating n-type semiconductor |
| C''' | cost by volume ($\$/\text{m}^3$) | opt | subscript designating optimum value |
| C'' | cost by area ($\$/\text{m}^2$) | p | subscript designating p-type semiconductor |
| C_B | bulk raw material cost ($\$/\text{kg}$) | P_{gen} | generator electric power output (W) |
| C_e | price of electricity ($\$/\text{kWh}$) | P_{sup} | electrical power supplied (W) |
| C_{HX} | heat exchanger cost ($\$/(\text{W}/\text{K})$) | Q_C | heat transferred through cold side heat exchanger (W) |
| $C_{M,B}$ | manufacturing cost to process bulk material ($\$/\text{kg}$) | Q_H | heat transferred through hot side heat exchanger (W) |
| $C_{M,A}$ | manufacturing cost to process material by area ($\$/\text{m}^2$) | Q_{TE} | heat transferred through legs (W) |
| COP | coefficient of performance | Q_{ll} | heat transferred between legs (W) |
| F | fill factor | r | amortization (discount) rate (h^{-1}) |
| G | generator cost-performance metric ($\$/\text{W}$) | R | electrical resistance (Ω) |
| G_{min} | minimum cost for thermoelectric device ($\$/\text{W}$) | R_L | electrical load resistance (Ω) |
| G_0 | cost-performance scaling metric for thermoelectric device ($\$/\text{W}$) | S | Seebeck coefficient (V/K) |
| H | cooler operating cost ($\$/\text{kWh}$) | S_{pn} | difference in Seebeck coefficients of p- and n-type legs (V/K) |
| I | electrical current (A) | T | temperature (K) |
| k | thermal conductivity (W/m-K) | T_C | cold side temperature (K) |
| K_C | thermal conductance of cold side heat exchanger (W/K) | T_H | hot side temperature (K) |
| K_H | thermal conductance of hot side heat exchanger (W/K) | T_m | mean junction temperature (K) |
| K_T | total thermal conductance (W/K) | T_1 | hot junction temperature (K) |
| K_{TE} | thermal conductance of thermoelectric legs (W/K) | T_2 | cold junction temperature (K) |
| K_{ll} | thermal conductance of parallel path (W/K) | ΔT | junction temperature difference (K) |
| L | leg length (m) | U | heat transfer coefficient of heat exchanger ($\text{W}/\text{m}^2 \text{K}$) |
| L_{DR} | diminishing returns optimum leg length (m) | ZT | module or material thermoelectric figure-of-merit |
| L_T | ratio of thermal conductivity to heat transfer coefficient of heat exchanger (m) | η | efficiency |
| | | ρ | density (kg/m^3) |
| | | σ | electrical conductivity (S/m) |

1. Introduction

Thermoelectric devices are used in power generation and cooling applications to either convert heat into electricity or to pump heat. To date, thermoelectric technology has been constrained to applications that include vehicle waste-heat recovery prototypes, space vehicle power sources, seat coolers, solid-state refrigerators, and temperature control in laboratory equipment. Thermoelectric conversion has received renewed interest due to the development of better-performing materials and their potential to improve the efficiency of combustion systems through waste-heat recovery [1–3]. Improvements in material performance are ongoing [4–6] since conversion efficiencies of typical thermoelectric materials remain below 10% [3,7].

Thermoelectric devices are attractive because they have no moving parts and can be silent, reliable, and versatile. Since multiple thermoelectric n- and p-type couples can be connected in series, a thermoelectric device can be smaller than a computer chip or larger than a solar panel. Nevertheless, considerable technical challenges remain. Existing thermoelectric converters have lower conversion efficiencies than alternatives such as organic Rankine cycles. While some applications are well established, in particular power sources for space vehicles, a variety of terrestrial applications – such as high temperature waste-heat recovery – are yielding new concerns about reliability and durability. Challenges related to sublimation, oxidation, thermal and electrical interface degradation, and thermal expansion mismatch remain critical for applications of thermoelectric devices [8–15].

Thermoelectric technologies face several additional commercialization challenges. The cost of many thermoelectric materials

may be prohibitively high, largely due to the use of tellurium and germanium in the most common contemporary thermoelectric applications [16]. Safety concerns preclude toxic materials such as lead [17]. The weight and specific power of thermoelectric devices are particularly important for mobile applications such as vehicle waste-heat recovery [18], yet few strategies for weight reduction have been proposed. While government funding for thermoelectric technology research and development has expanded significantly in the past decade, the relative lack of private sector familiarity with the technology made early stage financing for companies comparatively slow to follow [19]. There has been a rapid development of materials promising higher efficiencies, in many cases through the use of nanostructuring and novel crystal structures [1,4,6]. Recent prototypes demonstrated the feasibility of thermoelectric devices for widespread, terrestrial, scalable applications [20–23]. Multiple start-up companies have received recognition and funding while also forming partnerships with established academic and industrial research teams [15,18,24–26]. The continued development and deployment of scalable thermoelectric devices depend on the device cost and energy conversion performance [1,27].

There is an urgent need for a comprehensive assessment of the commercial feasibility of the most promising thermoelectric materials while also considering relevant manufacturing and system costs. Cost-performance analyses of this type have been conducted for other energy technologies such as batteries and photovoltaics by considering material extraction costs [28,29]. For thermoelectric devices, there have been multiple evaluations of the coupled thermal and electrical module performance without considering cost [30,31]. The importance of cost was considered by

normalizing the material figure of merit by the raw material cost, and the costs for specialized applications such as a marine waste incinerator have also been determined [17,27,32,33]. A method for determining cost using the thermal energy cost and the module construction cost for specified material thicknesses has been presented [32]. A recent investigation of the cost-efficiency trade-offs of thermoelectric generators first determined the geometry that optimizes the thermal and electrical performance of the

device and then calculated the material cost associated with the optimized dimensions [27]. The work highlighted the importance of optimizing modules in conjunction with the heat source and sinks in the overall system. An important extension to the optimization approach is made by evaluating the coupled thermal, electrical, and economic factors simultaneously [34]. This method captures the ability of a moderately efficient device with low capital cost to perform better in the market than a highly efficient

Table 1

Material identification table. Material type is indicated in the first column and by material name color coding: red for chalcogenides and SiGe, blue for silicides, purple for clathrates, green for skutterudites, black for oxides, yellow for half-Heuslers, and grey for others. (For interpretation of the references to color in this table caption, the reader is referred to the web version of this paper.)

| Material type | ID # | Material name | Manufacturing type | Material cost (\$/kg) | Evaluated for low or high temp. scenario | | | | Ref. |
|------------------------|------|---|--------------------|-----------------------|--|------------------|-----------------------|----------------|---------|
| | | | | | ZT _m material | F _{opt} | L _{opt} (mm) | Scenario Temp. | |
| Chalcogenides and SiGe | 1 | Bi ₂ Te ₃ | Bulk | 110 | 0.74 | 0.18 | 4.53 | Low | [35,36] |
| | 2 | Bi _{0.52} Sb _{1.48} Te ₃ | Bulk | 125 | 1.05 | 0.21 | 4.41 | Low | [37] |
| | 3 | Bi _{0.52} Sb _{1.48} Te ₃ | Nanobulk | 125 | 1.52 | 0.29 | 3.47 | Low | [37] |
| | 4 | Bi _{0.54} Te _{0.46} | Nanowire | 84 | 0.02 | 0.07 | 1.10 | Low | [38] |
| | 5 | (Na _{0.0283} Pb _{0.945} Te _{0.9733})(Ag _{1.11} Te _{0.555}) | Nanobulk | 81 | 1.45 | 0.34 | 3.01 | High | [39] |
| | 6 | Bi-doped PbSe _{0.98} Te _{0.02} /PbTe | Superlattice | 55 | 1.96 | 0.02 | 0.31 | Low | [40] |
| | 7 | AgPb ₁₈ SbTe ₂₀ | Bulk | 84 | 1.31 | 0.26 | 3.59 | High | [41] |
| | 8 | SiGe | Bulk | 679 | 0.30 | 0.07 | 2.66 | High | [42] |
| | 9 | Si ₈₀ Ge ₂₀ | Nanobulk | 371 | 0.53 | 0.13 | 3.39 | High | [42] |
| | 10 | SiGe | Nanowire | 679 | 0.22 | 0.06 | 1.59 | Low | [43] |
| Silicides | 11 | Mg ₂ Si _{0.85} Bi _{0.15} | Nanobulk | 6.67 | 0.67 | 0.74 | 29.5 | High | [44] |
| | 12 | Mg ₂ Si _{0.6} Sn _{0.4} | Bulk | 4.04 | 1.05 | ~1 | 45.5 | High | [45] |
| | 13 | Si | Nanobulk | 3.09 | 0.21 | 0.71 | 94.5 | High | [46] |
| | 14 | Si | Nanowire | 3.09 | 0.72 | 0.09 | 3.38 | Low | [47] |
| | 15 | MnSi _{1.75} | Bulk | 1.46 | 0.05 | ~1 | 37.5 | Low | [48] |
| | 16 | Mn ₁₅ Si ₂₈ | Nanobulk | 1.51 | 0.07 | ~1 | 35.7 | Low | [48] |
| Clathrates | 17 | Ba ₈ Ga ₁₆ Ge ₂₈ Zn ₂ | Bulk | 615 | 0.48 | 0.13 | 1.50 | High | [49] |
| | 18 | Ba ₈ Ga ₁₆ Ge ₃₀ | Bulk | 644 | 0.36 | 0.11 | 1.65 | High | [50] |
| | 19 | Ba ₇ Sr ₁ Al ₁₆ Si ₃₀ | Bulk | 1.64 | 0.09 | ~1 | 38.6 | High | [51] |
| Skutterudites | 20 | CeFe ₄ Sb ₁₂ | Bulk | 37 | 0.77 | 0.28 | 8.34 | High | [52] |
| | 21 | Yb _{0.2} In _{0.2} Co ₄ Sb ₁₂ | Bulk | 24 | 0.93 | 0.31 | 10.6 | High | [53] |
| | 22 | Ca _{0.18} Co _{3.97} Ni _{0.03} Sb _{12.40} | Bulk | 13 | 0.77 | 0.39 | 17.6 | High | [54] |
| Oxides | 23 | (Zn _{0.98} Al _{0.02})O | Bulk | 2.30 | 0.08 | 0.48 | 58.6 | High | [55] |
| | 24 | Ca _{2.4} Bi _{0.3} Na _{0.3} Co ₄ O ₉ | Bulk | 30 | 0.13 | 0.43 | 7.17 | High | [56] |
| | 25 | InGaZnO | Nanowire | 511 | 0.07 | 0.04 | 1.59 | Low | [39] |
| Half Heuslers | 26 | Na _{0.7} CoO _{2-δ} | Bulk | 36 | 0.52 | 0.22 | 12.7 | High | [57] |
| | 27 | Zr _{0.25} Hf _{0.25} Ti _{0.5} NiSn _{0.994} Sb _{0.006} | Bulk | 9.71 | 1.38 | 0.49 | 19.6 | High | [58] |
| | 28 | Zr _{0.5} Hf _{0.5} Ni _{0.8} Pd _{0.2} Sn _{0.99} Sb _{0.01} | Bulk | 8.51 | 0.69 | 0.46 | 15.4 | High | [59] |
| Other | 29 | Ti _{0.8} Hf _{0.2} NiSn | Bulk | 10.70 | 0.41 | 0.41 | 16.5 | High | [60] |
| | 30 | PEDOT:PSS | Polymer | 0.34 | 0.01 | ~8 | 101 | Low | [61] |

*See Table 2 below for scenario values.

1: Materials with F_{opt} ~ 1, have high thermal conductivities which suggests that heat exchangers with larger U-values should be used.

8: The cost of polymers and their manufacturing technique are so different from other thermoelectric materials that a different geometry than conventional TE should be considered.

Table 2

Scenario parameters, device temperatures, U-values, and heat exchanger (HX) costs. Representative applications are provided for each temperature scenario.

| Applications | Thermoelectric cooling | Low temperature recovery | Solar thermal generator | Automotive exhaust heat recovery | Industrial furnace heat recovery |
|--|------------------------|--------------------------|-------------------------|----------------------------------|----------------------------------|
| Scenario temperature | (Cooling) | Scenario #1 | Scenario #2 | Scenario #3 | Scenario #4 |
| | | Low | Medium-Low | Medium-High | High |
| Hot side temperature, T _H (°C) | 15 | 100 | 250 | 500 | 800 |
| Cold side temperature, T _C (°C) | 5 | 20 | 20 | 50 | 50 |
| Average temperature, T _m (°C) | 10 | 60 | 135 | 275 | 425 |
| Hot side U-value, U _H (W/m ² K) | ∞ | 102 | 102 | 120 | 120 |
| Cold side U-value, U _C (W/m ² K) | ∞ | 105 | 105 | 105 | 105 |
| HX & Plate Costs (\$/(W/K)) | – | 18.48 | 18.48 | 18.48 | 18.48 |

device with higher capital cost. While this prior work made progress on coupling efficiency and cost, the actual values and thus large impacts of manufacturing costs and the costs of key system components have not been considered. This is particularly important for the newer bulk and thin film materials for which manufacturing costs can be high, and new system designs might be required to optimize heat exchange.

The present work provides a detailed investigation of the materials, manufacturing, and system costs for 30 leading thermoelectric materials [35–61] considering the conversion efficiency. We combine these using cost metrics that account for the coupled cost and system design implications and trade-offs [34]. These metrics enable an assessment of which materials are most promising for heat recovery and cooling and incorporate an optimization of material thickness and fill factor. The present work sets targets for thermoelectric cooling and power generation. The cost of power generation, in \$/W, is reported by combining material properties, device physics, and raw material costs, all of which are reported for seven material classes presented in Table 1 and in Appendix F. The analysis is performed for five operating temperatures shown in Table 2 to reflect the myriad of potential thermoelectric applications. The difference in manufacturing costs for bulk and thin film materials influences the decision on whether to use novel materials. A comparison to existing, competitive technologies highlights the cost of current state-of-the-art thermoelectric technologies and device performance.

2. Methods

This work determines the appropriate device geometry based on cost and performance. The fill factor, F , and the leg length, L , of

a thermoelectric device are the dominant design parameters. The fill factor is the ratio of the area covered by the active thermoelectric material to the plate area, A , as illustrated in Fig. 1. While it goes against traditional thermoelectric module architecture, it is possible to envision devices with $F > 1$ (see Section 3.1). The inverse of the fill factor is known as the thermal concentration factor [62]. By reducing the fill factor, less active material is used, and the overall cost of the device can be reduced. In many applications, the fill factor is fixed to be above some minimum by other system constraints (e.g., mechanical robustness, voltage/areal requirements). By reducing the leg length at this fixed fill factor, less material is used, and the cost decreases. However, for a fixed heat exchanger and fixed F , as the thermoelectric leg length is reduced below some optimum, the temperature drop across the device decreases, and the output power decreases. This competition between power output and material volume suggests the existence of an optimum geometry which minimizes cost and maximizes power output. Therefore, the most appropriate metric for thermoelectric generators should be expressed on a \$/W basis as

$$G = \frac{C}{P_{gen}}, \quad (1)$$

where P_{gen} is the electric power output of the generator, and C is the capital cost of the device. The capital cost includes the material, manufacturing and heat exchanger costs which are described in detail in Section 2.2. Cost of the heat available for conversion is excluded. The contribution of heat exchanger and insulating ceramic plate costs are considered in Section 3.2. Both C and P_{gen} are strongly dependent on L and F . A cost-performance optimization should be performed on G rather than on C or P_{gen} individually [34].

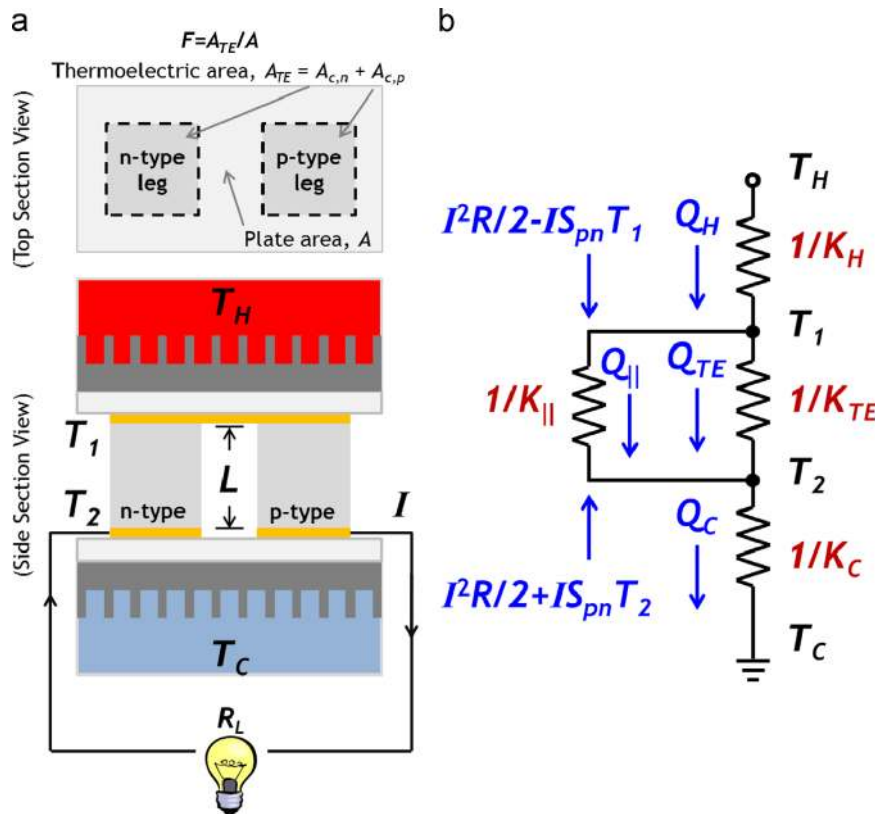


Fig. 1. Diagram of thermoelectric module and the equivalent thermal circuit. The n- and p-type thermoelectric materials are connected electrically in series with a metal (shown in orange). The thermoelectric legs are thermally in parallel between electrically insulating ceramic plates (shown in light grey). The analysis is conducted for constant hot- and cold-side temperatures T_H and T_C . There are two thermal conductance terms between the junction temperatures T_1 and T_2 representing heat transfer through the thermoelectric material legs and in the gap between the legs. The internal heat generation term, $I^2R/2$, is the Joule heating component; the Peltier term is $IS_{pn}T$.

A similar argument can be made for thermoelectric coolers. In order to reduce the capital cost of the module, shorter leg lengths are used. However, this reduces the efficiency of the thermoelectric cooler. Since thermoelectric coolers consume electricity and provide a cooling service, the cost of electricity is important, so a thermoelectric module with a large coefficient of performance, COP, is desirable. The COP is the ratio of the cooling power removed from the cold side to the electric power consumed. Electricity is purchased on a \$/kW h_e basis, so the most appropriate metric is the operating cost expressed in units of \$/kW h_{th} where the subscripts represent electric and thermal (cooling) energy, respectively. The capital cost of the thermoelectric cooler is amortized over the lifetime and added to the operating cost. Operating continuously and purchasing electricity hourly over the lifetime allows for a simplification in the amortization where the capital cost is multiplied by the amortization (discount) rate, r , on an hourly basis (see Appendix B). This allows for both capital cost and operating costs to be considered for cooling applications. The appropriate operating cost metric is

$$H = \frac{C_e}{\text{COP}} + r \frac{C}{\text{COP} \cdot P_{\text{sup}}} \quad (2)$$

where C_e represents the price of electricity, and P_{sup} is the electric power supplied to the device to maintain a desired temperature difference across the module. The price of electricity varies. In the United States, the average industrial user purchases electricity at a price of \$0.068/kW h_e, and residential users purchase electricity at a price of \$0.12/kW h_e. The average price of electricity is taken as \$0.098/kW h_e in this analysis and is bounded by the industrial and residential prices (*i.e.*, the error bars). These values are the average U.S. electricity prices reported by the Energy Information Agency at the time of article submission. The product of the COP and P_{sup} is the thermal cooling power, in kW_{th}, and yields the thermal energy removed in kW h_{th} once divided by r .

2.1. Device physics

Both of these cost metrics rely on first modeling the physics of the thermoelectric device. Fig. 1 depicts a dual-leg thermoelectric module with the legs connected electrically in series and thermally in parallel. The electrical and thermal transport for this geometry has routinely been solved [30,63–66]. The total thermal conductance of the thermoelectric module, K_T , is the sum of the thermal conductance through the active material, K_{TE} , and a parallel thermal leakage conductance, K_{\parallel} . The heat transferred between the legs, Q_{\parallel} , is described by K_{\parallel} which is the sum of conduction, convection, and radiation contributions. For most applications, conduction is the dominant heat transfer mechanism, but radiation and convection can be significant. As a result of these three contributions, K_{\parallel} and K_T are non-linear functions of leg length L . A description of how K_{\parallel} is handled in this analysis can be found in Appendix D. The heat flowing through the thermoelectric legs, Q_{TE} , is augmented by the Joule heating distributed throughout the thermoelectric legs and Peltier cooling/heating that occur locally at the hot and cold junctions.

In addition to the thermal conductance of the module, the thermal conductance of the hot- and cold-side heat exchangers, K_H and K_C , respectively, strongly influence the overall device performance. These conductances are further reduced by any series temperature drops due to the electrically insulating ceramic plates and module thermal contact resistances. The effect on device performance from the heat exchangers has been considered [67]. In this analysis, the contribution from the metallization, ceramic plates, and heat exchangers is also considered, and details can be found in Appendix D. The values of the thermal conductances are dependent on the application and heat exchangers (*i.e.*, reservoir

temperatures and working fluids). The U -value of the heat exchangers and the thermal conductance are related to each other by the heat transfer area, $K=UA$, and the values [68] used in this analysis along with application reservoir temperatures are summarized in Table 2. For the scenarios selected in this analysis, the appropriate hot side and cold side exchangers have approximately the same U -value, so matched heat exchanger simplifications (*i.e.*, $K_H=K_C=K$) are appropriate. However, for exactness these simplifications are not used in this analysis. Ultimately, these series conductances relate the hot- and cold-side reservoir temperatures, T_H and T_C , to the hot-side and cold-side junction temperatures, T_1 and T_2 .

2.1.1. Power generation

The temperature difference governs the energy that can be converted into a thermoelectric generator. For the electrical load matched condition, energy balances of the device at the hot and cold junctions yield a system of coupled non-linear equations:

$$K_H(T_H - T_1) - K_T(T_1 - T_2) - \frac{S_{pn}^2(T_1 - T_2)T_1}{2R} + \frac{S_{pn}^2(T_1 - T_2)^2}{8R} = 0 \quad (3a)$$

$$\frac{S_{pn}^2(T_1 - T_2)^2}{4R} - K_H(T_H - T_1) + K_C(T_2 - T_C) = 0, \quad (3b)$$

which can be solved numerically for the exact junction temperatures. In this expression, $S_{pn}=S_p-S_n$ is the difference in thermopowers of the two legs, and R is the internal electrical resistance of the module. Under the approximations that the electrical contact resistance, metallization, and shunt resistances are negligible, and the thermoelectric legs have the same electrical conductivity $\sigma_p=\sigma_n=\sigma$, the internal electrical resistance is $R=4L/(\sigma AF)$. The analysis is conducted assuming the properties are constant within each of the five temperature ranges considered, and the properties are evaluated at the mean of the reservoir temperatures (*i.e.*, $T_m=(T_H+T_C)/2$). Thermal and electrical contact resistances are not considered as these vary widely and are unique to each device; they are most important for short leg lengths, typically < 1 mm. These effects can significantly reduce the performance of a device, but neglecting these terms provides a lower (optimistic) bound on the \$/W cost determined for each material.

The amount of power converted by a thermoelectric generator is

$$P_{\text{gen}} = \frac{S_{pn}^2(T_1 - T_2)^2}{R} \frac{m}{(m+1)^2}, \quad (4)$$

with

$$m = \frac{R_L}{R} \quad (5)$$

as the ratio of the load resistance, R_L , to the internal electrical resistance, R , of the module. The thermoelectric generator can be operated at maximum power when $m=1$ (*i.e.*, load matched) or at maximum efficiency when $m=\sqrt{1+ZT_m}$. It has been recently reported that, due to thermal feedback from the load resistance (*e.g.*, increasing the load resistance increases the junction temperatures difference slightly), m should be slightly greater than these nominal values [31,69]. While this is strictly true, the effect is a higher order correction, and traditional analysis [30,31] suggests that one of these m conditions should be selected. The value of m that minimizes the \$/W is $m=1$ because this condition maximizes the denominator of Eq. (1). Therefore, the load resistance is set to exactly equal the internal resistance [34].

In this work, ZT is the *module* figure-of-merit

$$ZT \equiv \frac{S_{pn}^2 T}{K_T R} \quad (6)$$

and $T_m=(T_1+T_2)/2$ is the average of the junction temperatures. Eq. (6) is similar to the material figure of merit $ZT=S^2\sigma T/k$, with the material's thermopower, S , electrical conductivity, σ , and thermal conductivity, k . The module and material ZT are related as discussed in Appendix A. For this manuscript, the material ZT will be used to identify the materials in the figures while the module ZT is used in the analysis under the simplification that the n- and p- type legs have the same thermopower magnitude, same electrical conductivity, and same thermal conductivity.

Using the electric power and the cost of the device, Eq. (1) can be evaluated in units of \$/W as a function of L for a chosen F as shown in Fig. 2a for a doped bismuth telluride example (Material ID #2). By selecting a fill factor, an optimum length, L_{opt} , exists which minimizes G . The heat flowing into the hot side, Q_H , and the thermal efficiency, $\eta=P_{ge}/Q_H$, are determined as a function of leg length as shown in Fig. 2b. Using Eqs. (3)–(5), the electric power generated is determined as a function of leg length as shown in

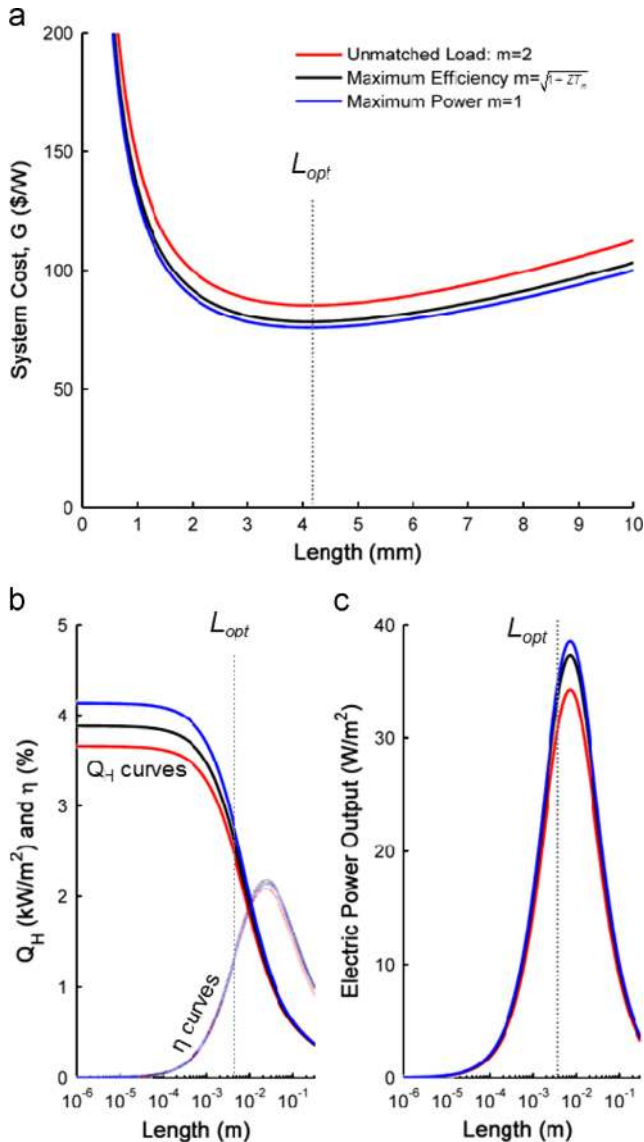


Fig. 2. Example of optimum leg length L_{opt} and cost G minimization for power generation using Material ID #2 in Table 1 (bulk $\text{Bi}_{0.52}\text{Sb}_{1.48}\text{Te}_3$) with $F_{opt}=0.21$ and parameters in the low temperature scenario of Table 2. The leg length that results in the minimum cost (a, $L_{opt}=4.4$ mm) is not the same length that maximizes the efficiency (b, $L_{max,\eta}=24$ mm) or output power (c, $L_{max,p}=7.3$ mm). Note (a) is on a linear scale while (b) and (c) are on a log scale. The black and blue η curves in (b) are nearly indistinguishable. (For interpretation of the references to color in this figure caption, the reader is referred to the web version of this paper.)

Fig. 2c. The leg length which minimizes G is different from the leg length that maximizes efficiency or the leg length that maximizes the electric power output. Fig. 2 shows the difference between designs optimized for efficiency or power and an alternative design that optimizes the ratio of cost to power output.

The cost, efficiency, and electric power output are functions of the load condition m as discussed in Appendix A and as illustrated by the different color lines in Fig. 2. In situations where there is excess heat (i.e., fuel/heat is free) the maximum power condition $m=1$ is most appropriate and yields the lowest cost. In situations where heat is costly, the maximum efficiency condition may be more appropriate. Evaluating fuel costs is beyond the scope of this work but has been investigated elsewhere [32]. The unmatched condition (i.e., m is arbitrary) may also be acceptable depending on the application or cost of power electronic conditioning circuits necessary to load match.

Power electronic conditioning circuits match the resistance of the load to the resistance of the module in order to maintain either the maximum power condition ($m=1$) or the maximum efficiency condition ($m=\sqrt{1+ZT_m}$). The cost-necessity of these circuits is evaluated in Fig. 3. The lack of a proper load condition results in an opportunity cost for power generation which is plotted as a function of ZT_m . The opportunity cost is expressed as a percentage of the capital cost of the device. The $m=1$ (horizontal blue line) case is the ideal situation where there is no opportunity cost. Other arbitrary load conditions (horizontal red lines) represent different degrees of opportunity costs. The black curve in Fig. 3 is the percent difference between G with $m=\sqrt{1+ZT_m}$ and G with $m=1$; this is the opportunity cost for operating at the maximum efficiency condition rather than the load matched condition. The black circles represent the position of materials considered in this study along the maximum efficiency line. For most materials in this study, ZT_m is low enough that operating at the maximum efficiency or maximum power makes little difference. However, at larger ZT_m this difference becomes significant. For a device operating at a condition other than $m=1$, the opportunity cost is higher, and the added cost of power electronics should be considered. For example, if a material has a $ZT_m=1$, and throughout normal

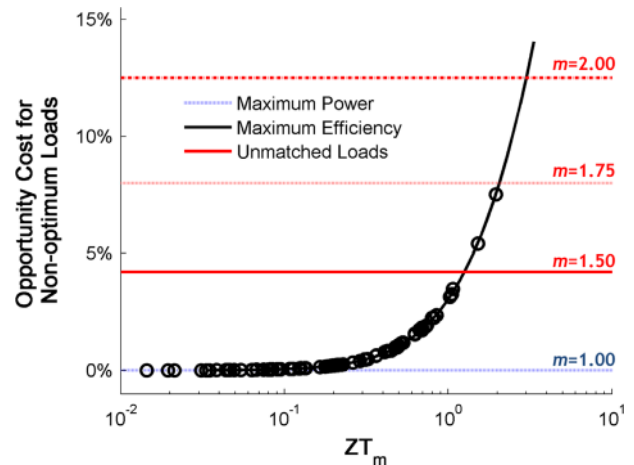


Fig. 3. Cost associated with non-optimized load conditions. The opportunity costs are percentages of the total capital cost of the module. Designing a power electronics conditioning circuit to load match has appreciable cost benefit. The horizontal lines represent specific load conditions $m=R_L/R$: (blue, $m=1$) maximum power condition (black, $m=\sqrt{1+ZT_m}$), maximum efficiency condition (red, $m=1.50, 1.75, 2.00$) unmatched load conditions. The circles represent the practical maximum efficiency conditions of the materials investigated in this study. The optimum load is the matched load ($m=1$), which produced the maximum power and the zero opportunity cost. (For interpretation of the references to color in this figure caption, the reader is referred to the web version of this paper.)

operation m fluctuates to 1.5 for a large fraction of generating time, then an opportunity cost of 4% of the capital cost is incurred in the absences of conditioning circuits. If the conditioning circuit costs less than 4% of the capital cost of the device, then the additional power delivered warrants the cost of the conditioning circuit. This varies with each material/system as they have different capital costs. For inexpensive systems the additional system cost of conditioning circuits is not justified whereas this cost may be justified for expensive systems.

2.1.2. Levelized cost of energy considerations

The levelized cost of energy (LCOE) is often used to compare the value of different energy generating technologies; a lower LCOE value corresponds to a lower cost to generate electricity [70]. This metric is a function of several variables including the overnight capital cost, the ongoing fuel costs, and the recurring maintenance costs. These costs are spread over the lifetime of the system at a specified capacity factor (uptime) and financial discount rate. The units of LCOE are typically \$/kWh, and determining the LCOE value is application-specific because of the number (and specificity) of input parameters. The analysis in this manuscript only calculates the overnight capital cost of the generator (related to G), which is only one input parameter for the LCOE value. A simplified LCOE method is presented in Appendix C and provides a way of converting the \$/W value into a \$/kWh value using more specific parameters which are beyond the scope of this manuscript.

2.1.3. Thermoelectric cooling

The device physics of thermoelectric coolers are similar to those of generators except that electric power is supplied to support a temperature difference rather than being generated. It is usually desirable to operate thermoelectric coolers at the maximum COP since electricity is continually purchased. For thermoelectric cooling the goal is to maintain a specified temperature difference at the junctions of the module. The hot- and cold-side heat exchangers act as additional thermal resistances. The cold-side junction T_2 needs to be colder than T_C , and the hot side junction T_1 needs to be hotter than T_H . This over cooling/heating places an extra burden on the thermoelectric module design as the cold side junction needs to be cooled below the target reservoir temperature. Removing this burden for simplification, ideal hot side and cold side heat exchangers are considered here (i.e., $U = U_H = U_C = \infty$). However, the series thermal resistances of the ceramic plates and metal shunts are still included, so K_H and K_C are finite (see Appendix D). This simplification fixes the temperature of the exteriors of the ceramic plates to be the reservoir temperatures. The fill factor F is approximately one because the device should be covered in as much active thermoelectric material as possible in order to pump heat.

Under these simplifications ($U = \infty, F = 1$), the mean junction temperature is approximated as the mean reservoir temperature, $T_m \approx (T_H + T_C)/2$, enabling an explicit solution for the junction temperatures by performing an energy balance on the cold side junction. This yields a quadratic equation:

$$\left(\frac{S_{pn}^2 \sqrt{1+ZT_m}}{R(\sqrt{1+ZT_m}-1)^2} \right) T_2^2 + \left(\frac{S_{pn}^2 T_m \sqrt{1+ZT_m} + 1}{R(\sqrt{1+ZT_m}-1)^2} + K_T + \frac{K_C}{2} \right) T_2 + \left(\frac{-S_{pn}^2 T_m^2}{R(\sqrt{1+ZT_m}-1)^2} - K_T T_m - \frac{K_C T_C}{2} \right) = 0 \tag{7}$$

for which the smallest root is the cold side junction temperature, and the hot side junction temperature is determined using

$T_1 \approx 2T_m - T_2$. These junction temperatures are used to determine the COP and supplied power P_{sup} :

$$COP = \frac{T_2}{T_1 - T_2} \left[\frac{\sqrt{1+ZT_m} - T_1/T_2}{\sqrt{1+ZT_m} + 1} \right] \tag{8}$$

$$P_{sup} = \frac{2S_{pn}^2 (T_1 - T_2)^2}{R(\sqrt{1+ZT_m} - 1)} \tag{9}$$

Both of these equations are functions of leg length and can be evaluated numerically. Finally, using these equations, the operating cost of thermoelectric cooling, H in Eq. (2), can be evaluated.

2.2. Cost considerations

In addition to the device physics, both material and manufacturing costs influence the overall cost metric. The cost, C in Eqs. (1) and (2), is a function of the bulk raw material cost C_B (\$/kg) as summarized in Table 1. The manufacturing cost associated with processing bulk material $C_{M,B}$ (\$/kg), the areal manufacturing cost $C_{M,A}$ (\$/m²), and the cost of both heat exchangers C_{HX} (\$/(W/K)) are found in Table F.2 in Appendix F. The overall cost C is also dependent on the heat exchanger heat transfer coefficient U , the density of the active material ρ , the leg length, and area of the ceramic plates, A :

$$C = \left(\underbrace{(C_B + C_{M,B})\rho L}_{C'''} + \underbrace{C_{M,A}}_{C''} \right) AF + C_{HX} UA \tag{10}$$

The collection of terms in the first expression is a volumetric cost C''' (\$/m³), and the second term is an areal cost C'' (\$/m²), both of which include manufacturing costs. These costs are determined based on a conceptual estimating technique [71] since these devices are largely unprecedented. This technique projects costs for future products which do not exist rather than gathering prices for components of a device already in production. Rapid iterations on cost estimates completed in tandem with thermoelectric product development will prove valuable as devices enter the market.

The cost of the extracted raw, bulk material C_B captures the fundamental differences in material costs. The material cost is determined from the 2011 price of each element as reported by the U.S. Geological Survey; it is based on the worldwide production of the element and represents the average price an industrial consumer would pay [72]. Thermoelectric materials are typically composed of raw materials which have been processed to a purity level of 99% or higher [16]. Typical costs for pure materials are presented in Appendix F and can be significantly higher than the raw material cost. For instance, aluminum is an abundant material with a raw material cost of \$2.60/kg. However, the cost of 99.999% pure aluminum is approximately \$300/kg [73]. While purification adds to the material cost [16], the cost of purified materials is highly uncertain. It can vary significantly by vendor and is strongly influenced by rapidly changing market and processing factors [14,59,74,75]. This volatility can convolute the cost-performance analysis, so the cost to purify materials is omitted here without biasing the results since the purification conditions apply to most minerals [29]. A comparison between pure material and raw material costs was conducted, and the relative cost differences between each material and their subsequent ranking did not change when pure material costs were considered.

Manufacturing costs are divided into two categories based on the method of material processing. Processes enacted on the entire bulk volume of material such as ball milling and spark plasma sintering have costs denoted by $C_{M,B}$. Other processes like dicing and metallization depend on the area of material processed; these

costs are indicated by C_{MA} . The cost is calculated by dividing the equipment capital cost by the equipment lifetime and throughput. The exact cost and throughput values are available in Appendix F. In most cases, the cost and throughput of equipment were obtained from quotes or estimates provided by equipment vendors. Throughput is highly dependent on the specific application and product, so it is not easily generalized to a variety of materials and applications. An activity measure [71] has been assigned to the manufacturing equipment considered here which assumes the equipment will be in operation year-round. A 20-year equipment lifetime and 24 h per day, 365 days per year operation were assumed. This approach considers the total equipment effectiveness [76] and provides the lower bound on manufacturing cost. An overall equipment effectiveness which incorporates equipment shutdown for issues like repair and maintenance could also be considered [76]. The effect on the results presented here are minimal for realistic overall equipment effectiveness values. When the analysis is conducted assuming equipment operation for 75% of the year, the resulting increase in the cost metric G is $\sim 5\%$ or lower for most materials. The exception is the superlattice material (Material ID #6) for which the increase is $\sim 10\%$. Additional costs of tooling, maintenance, repair, assembly (automated or manual), overhead, and labor are not included in this analysis.

The required throughput of thermoelectric material in a manufacturing process will depend on both the performance of the material and the yield of the process. Fewer legs will be required for higher thermopower materials, and less material must be processed as yield improves. The amount of active material consumed may be different than the amount of active material in the final device due to material losses during manufacturing processes. For instance, material can be lost during dicing processes, deposited on chamber walls during deposition, or removed through etching. The impact of any fractional loss of the material on the end cost would be the same as any changes made to the equipment effectiveness as described above. A description of how to adjust the manufacturing cost for this fractional loss is provided in the Appendix F. In order to provide the lower bound for cost, the results reported neglect the additional cost of material lost due to manufacturing processes.

Manufacturing equipment costs are approximate and estimated for new equipment. Equipment is typically tailored specifically for the end-use application, so communication with vendors is required for accurate quotes and precise costs. Particularly in early stage research, development, and production, tools built in-house or used/refurbished equipment may be used to reduce costs. In some cases, it may be more cost effective to use a service provider or user facility for certain manufacturing steps rather than purchasing equipment and performing the process in-house [36,77,78]. Equipment and manufacturing costs used herein serve as points of reference; real manufacturing costs vary by material, process, and application.

Table 1 summarizes the state-of-the-art materials with published and peer-reviewed thermoelectric properties used in the analysis. They are from the following classifications: chalcogenides, silicides, clathrates, half Heusler alloys, skutterudites, and oxides. A novel polymer material, PEDOT:PSS, has recently been proposed for thermoelectrics and is also included here [61]. The areal manufacturing costs associated with the polymer material are unique since a polymer device would likely be made using a process like screen printing. A solution printing process can also be used for the metallization layer in these cases, eliminating the need for dicing. Hence, C_{MA} for polymer or solution-processed materials could be significantly lower than other materials.

Both bulk and film materials are considered with the latter referring to thin film, superlattice, and nanowire materials. The raw material cost for each thermoelectric material is also reported

in Table 1 along with the references for material properties and characterization results. Materials are also designated by their manufacturing class: bulk, nanobulk, nanowire, superlattice, and polymer. Nanobulk materials are ones which were identified by the original authors as having nanoscale grain structures.

The limitations of manufacturing techniques in turn limit the achievable range of leg lengths. If the optimum leg length based on the cost-performance optimization lies outside the manufacturing limits, entirely new manufacturing methods would have to be developed at a significant additional manufacturing cost. Bulk materials should be limited to a minimum leg length of 500 μm as defined by dicing saw limits [79]; however, after executing the analysis none of the bulk materials selected for this study approached this dicing limit. Furthermore, no leg length limitation was placed on nanowire materials since nanowires shorter than 500 μm can be fabricated, and there is no inherent manufacturing limitation to making long thermoelectric legs with nanowires. The intrinsic, single-nanowire material properties reported in the references considered here may be different than a geometry with multiple nanowires, but those considerations are case-specific and beyond the scope of this analysis.

Potential thermoelectric power generation applications span a large range of operating temperatures. Therefore, the analysis was conducted for five operating temperatures representing various proposed applications as shown in Table 2. Temperature-dependent material properties were extracted from the references listed in Table 1, and the material properties at the mean reservoir temperature were used in the analysis.

2.3. Methods summary

Using the device physics models, material properties, material costs, manufacturing costs, and heat exchanger costs, the metrics G (Eq. (1)) for power generation and H (Eq. (2)) for thermoelectric cooling can be evaluated for a variety of traditional and novel thermoelectric materials. In its complete form, G is expressed as [34]

$$G = \frac{4}{S_{pn}^2 \sigma (T_1 - T_2)^2} \left(\frac{(m+1)^2}{m} \right) \left(C'' L^2 + C'' L + \frac{C_{HX} U L}{F} \right), \quad (11)$$

where the junction temperature difference is evaluated numerically by solving a non-linear system of coupled equations (Eqs. (3a) and (3b)). A point of diminishing returns in system cost exists which designates the optimum fill factor, F_{opt} [34]. The true minimum occurs when F or L is zero. This point is unrealistic as no device would exist. Therefore, the diminishing returns point nearly minimizes G . The diminishing returns optimum point is

$$L_{DR} = \sqrt{\frac{k C_{HX}}{C''}}, \quad F_{opt} = \frac{1}{2} \sqrt{\frac{C_{HX} U^2}{C'' k}}. \quad (12)$$

By fixing F at this diminishing returns value, F_{opt} , an optimum L exists that uniquely minimizes G , designated as L_{opt} . We present both the $F=F_{opt}$ and $F=1$ scenarios which provide the optimized system costs at an optimum L_{opt} given a fixed F .

The analysis provides a detailed derivation of a new cost-performance metric G_0

$$G_0 = \frac{16 C'' L_T^2}{S_{pn}^2 \sigma (T_H - T_C)^2}, \quad (13)$$

where L_T is the ratio of the material thermal conductivity, k , to the heat exchanger thermal conductance, U . G_0 is a characteristic scaling metric for G and accounts for material cost, application temperatures, heat exchanger performance, and thermoelectric material properties. For a fixed F , when the metal shunt, ceramic plate, heat exchanger, and manufacturing costs are excluded, the

resulting cost metric G_{min} is the minimum material cost for a thermoelectric device [34]:

$$G_{min} = 4G_0F^2 \quad (14)$$

The fill factor can equal F_{opt} or some other value as determined by device design requirements not considered in this analysis. This minimum material cost scales as F^2 ; so exceedingly small fill factors will allow for small material costs. For example, for Material #2 in the low temperature scenario with a fill factor of $F=0.01$ the minimum material cost is $G_{min}=\$0.0084/W$ which is two orders of magnitude smaller than the value reported in Fig. 5 with $F_{opt}=0.21$. This minimum represents the material cost dominated regime; however, other regimes where cost is dominated by either the areal manufacturing or the heat exchanger also exist [34] and have different minimums.

For cooling, the thermoelectric operating cost H is

$$H = \frac{C_e}{COP} + r \frac{C''L^2 + C'L}{\frac{1}{2}S_{pn}^2\sigma(T_1 - T_2)^2} \frac{\sqrt{1+ZT_m} - 1}{COP} \quad (15)$$

where the junction temperature difference and COP are determined by solving the quadratic in Eq. (7). In power generation and thermoelectric cooling, the thermal conductance of the device, the electrical resistance, and the overall cost are complex functions of the leg length L and fill factor F .

3. Results and discussion

The results specifically address the cost of candidate materials, the cost to process those materials into thermoelectric legs for a module, and the cost of the heat exchangers making up the full thermoelectric device. This enables realistic assessments of current and future materials' potential for use in power generation and cooling applications by linking performance with estimated material, manufacturing, and system costs.

3.1. Material and module manufacturing costs

The contribution of manufacturing, material, and heat exchanger costs differ by the manufacturing and material types. Fig. 4 depicts the cost for processing typical bulk, nanobulk, nanowire,

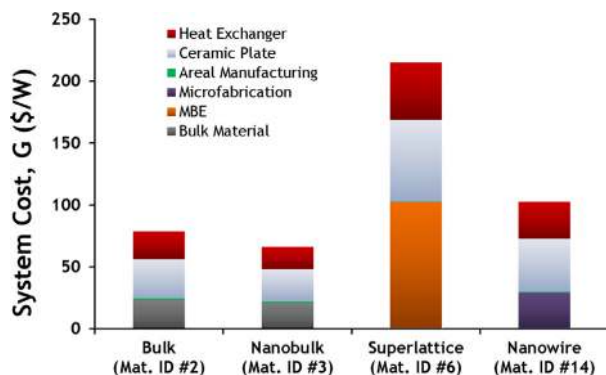


Fig. 4. Example system cost breakdown for various manufacturing classes on a \$/W basis. These values correspond to the $F=F_{opt}$ case in Fig. 5a. The low temperature case (Scenario #1) was used, and the cost was evaluated for the optimum fill factor and leg length ($F=F_{opt}$, $L=L_{opt}$) for each material. For nanowire materials, the value $\$2500/m^2$ approximating early production microfabrication cost was used in the analysis and corresponds to about $\$1/g$ for processing silicon. For the superlattice material, $\$1800/m^2$ corresponding to $\$40/g$ for processing lead telluride was used. Areal manufacturing cost (in green) represents the cost of dicing and the metallization of the thermoelectric material. The electrically insulating ceramic plate and heat exchanger costs are a substantial portion of the overall cost for all thermoelectric devices. (For interpretation of the references to color in this figure caption, the reader is referred to the web version of this paper.)

and superlattice thermoelectric materials for power generation. The numerical values and cost assumptions are presented in the Appendix F. A similar breakdown can be performed for thermoelectric cooling, but it is less interesting since the cost of electricity dominates. For power generation, the cost of the ceramic plates and heat exchangers are a dominant cost for most manufacturing classes. Although their contribution to the overall cost is substantial, heat exchangers can increase the device performance since they improve heat transfer to and from the hot and cold reservoirs. This analysis suggests that a major reduction in overall system cost can be achieved by making inexpensive heat exchangers ($< \$1.00/(W/K)$) with high U -values ($> 200 W/m^2 K$). Ceramic plates, typically used as substrates in planar thermoelectric modules, provide the necessary electrical insulation and mechanical support for the device and represent an important cost. A significant reduction in overall system cost could be achieved by making an inexpensive ($< \$0.10/cm^2$), thermally conducting ($k > 40 W/m K$), electrically insulating, and structurally suitable substrate material that can operate at the given application temperature.

The advantage of nanobulk materials is evident in Fig. 4 as illustrated with a nanostructured bismuth telluride material (Material ID #3) compared to the similar bulk material (Material ID #2). The nanobulk material has a lower thermal conductivity than its bulk counterpart, so it has a lower $\$/W$ value. By nanobulk processing, a hierarchy of length scales relevant for thermal and electrical transport can be engineered to produce a better thermoelectric material [80]. These processing techniques are still affordable and demonstrate the benefit of a slight increase in manufacturing cost that results in an overall reduction in the $\$/W$ value. This example demonstrates a $\sim 17\%$ overall cost reduction on a $\$/W$ basis.

Nanowire materials may require microfabrication processes like those used in semiconductor manufacturing. In semiconductor device manufacturing, cost typically scales with the number of fabrication steps involving lithographic patterning and etching, so there is a range in microfabrication costs. The minimum of this range corresponds to a high-volume process similar to the current state of silicon photovoltaic fabrication. The maximum of this range corresponds to multi-mask processes used to make complementary metal oxide semiconductor (CMOS) devices. In the middle cost range are fabrication steps that are used to make micro-electro-mechanical systems (MEMS); this is the cost used for nanowire manufacturing in this analysis.

Superlattices are made using molecular beam epitaxy (MBE) which requires many hours to deposit a typical thickness of material, so the cost associated with achieving sufficiently thick thermoelectric legs is high. Since the manufacturing costs associated with thin film materials are significantly higher than those for bulk materials, the increase in power output achieved by these materials must far outweigh the additional cost. Given the manufacturing cost of MBE, little active material is used as demonstrated by the small leg length in Table 1. For MBE grown materials, bulk material costs are low because little active material is used. The cost associated with material deposited on surfaces other than the active substrate is not considered here as described earlier in Section 2. Appendix F includes details regarding a method to adjust the manufacturing cost and compensate for a material loss factor.

Metallization and dicing costs are areal manufacturing costs; they are applied to all materials considered herein equally since both are required for the traditional approach of assembling individual legs into modules. The metallization category denotes the deposition of diffusion barriers and metallization to improve contact to the electrical shunt. This cost includes both the cost of the equipment and an approximate cost of the metal deposited. An important exception to traditional metallization and dicing

processes is the relatively novel polymer thermoelectric material processing. The metallization and formation of individual leg structures would likely be done entirely through screen printing processes or a similar process commensurate with the unique fabrication of polymers. The impact of this exception is evident in the final G values computed for this material where the heat exchanger cost is neglected, and the system parameters used are $L=100$ mm, $F=8$, $T_H=100$ °C. The screen printing approach would lead to an estimated polymer thermoelectric module cost of \$140/W as opposed to \$550/W if traditional metallization and dicing costs were applied.

Large mismatch in costs can yield interesting new results. Specifically, the inexpensive material and manufacturing costs associated with the polymer and its low thermal conductivity, results in an optimum fill factor greater than one. This occurs because the cost of the heat exchanger is much larger than the cost of the material (i.e., $C_{HX}U^2 \gg C''k$). While a fill factor greater than one does not adhere to traditional thermoelectric architecture, it is not unimaginable. This is simply the situation where the cross sectional area of the legs is larger than the plate area. This is the reverse of thermal concentration where heat is actually spread laterally through the leg. In this analysis, the same heat exchanger was used to compare all materials. This heat exchanger (primarily its cost) is not suitable for polymers. This analysis suggests polymers require different geometries and heat exchangers than traditional thermoelectrics.

3.2. Thermoelectric power generation

The cost-performance analysis for thermoelectric power generators demonstrates their cost competitiveness when using different thermoelectric materials. Table 1 provides an overview of the material types, gravimetric costs (\$/kg), properties, and optimal geometries. In this table, the optimal geometries and ZT are reported for a specific temperature application (identified in Table 2 and defined by either “low” or “high”) where that material performs best. Other temperatures will have a different optimum leg length and fill factor for each material. In some cases, particularly nanowire and superlattice materials (e.g., Material ID # 6 and 14), only low temperature material property data is available, but the optimal ZT values may be at higher temperatures.

There are complex interplays between the thermal transport properties, electrical transport properties, and costs that influence the thermoelectric leg length. For example, a low thermal conductivity material allows for shorter legs, which results in lower electrical resistances and lower volumetric costs. The consequence of high thermal conductivity is starkly illustrated by nanobulk silicon (Material ID #13) where the high thermal conductivity (> 10 W/mK) results in an optimum thermoelectric leg length of over 90 mm. A high electrical conductivity permits longer legs, which results in larger output power and lower \$/W cost. There are also complex interplays between manufacturing areal cost, heat exchanger cost, heat exchanger thermal conductance, and material thermal conductivity that influence the fill factor. For example, expensive materials favor small fill factors to reduce costs while low thermal conductivity materials favor larger fill factors. However, the fill factor is commonly fixed by other system constraints, and an optimal thermoelectric leg length is sought.

This optimum leg length is the length that minimizes the cost for a given fill factor (typically F_{opt}) and is determined for each material and temperature scenario. This optimum leg length is not the diminishing returns point in Eq. (12) but rather the true leg length that minimizes the system cost in Eq. (11) for a fixed fill factor. The optimum leg length is used to calculate the values reported in Figs. 4 and 5. Three fill factor cases are presented in Fig. 5 for each of the temperature scenarios. The first case is for

$F=1$, and the second case is evaluated at the optimum fill factor $F=F_{opt}$ (Eq. (12)). The last case is a minimum achievable cost where F is fixed at the same F_{opt} value as the second case (i.e., $G_{min}=4G_0F_{opt}^2$, when $K_{||}$ is negligible). This minimum cost is reached when the system costs of ceramic plates and heat exchangers (C_{HX}) as well as the metal shunts and manufacturing costs (C'') are eliminated, and only the material cost (C'') for the thermoelectric device is considered. The gap between this minimum cost case and the other cases represent the room for improvement in manufacturing and system costs.

While there are many materials that can operate at low temperatures for energy scavenging applications, their thermoelectric materials costs alone are above \$1/W (Fig. 5a). The materials with the lowest minimum cost for the low temperature scenario, $T_m=60$ °C, are predominately bismuth telluride-based chalcogenides (Material ID #1-3) although the bismuth telluride nanowire material (Material ID #4) has high costs. The presence of certain nanowire (Material ID #14) and superlattice (Material ID #6) materials at the bottom of the range presented for the minimum cost in Fig. 5a highlights the potential of nanostructured materials to also be cost competitive. However, the gap between the minimum cost points and the other cases indicates that the heat exchanger, ceramic plate, and areal manufacturing costs must be reduced (to $< \$1.00/(W/K)$, $< \$1.00/cm^2$, and $< \$0.01/cm^2$, respectively, see Section 3.4) for most thermoelectric materials to be competitive. One option to reduce manufacturing costs of nanomaterials may be to use solution-synthesized nanostructures since they do not require specialized microfabrication equipment and processes. Nanostructured bulk material made with processes like ball milling also have lower manufacturing costs than nanowire and superlattice materials. The combined effects of cost and performance are responsible for this result; the thermoelectric efficiency improvements outweigh the additional costs.

Certain materials are clearly promising for the mid- to high-temperature applications as shown in Fig. 5c. The lead telluride-based, half Heusler, skutterudite, and silicide materials designated by Material ID #5, 7, 27, 21, and 12, respectively, have consistently low costs ($< \$6/W$). In fact, a factor of two reduction in the system costs for these materials would make them highly competitive waste-heat recovery solutions as compared to Rankine or organic Rankine cycles at \$4–5/W, especially when factors such as installation costs, reliability, and maintenance are also considered. A notably high-cost material type is the oxide category (Material ID #23, 24). In spite of the low bulk material cost, the ZT_m is too low, largely due to the high thermal conductivity.

These results should be placed in perspective considering the costs of competing electricity generation technologies, especially with respect to the heat source temperature [7,81]. The horizontal lines in Fig. 5 indicate the cost of competing technologies. When the full optimization is performed, Fig. 5a–d shows that current thermoelectrics are primarily competitive for mid- to high-temperature applications. As shown in Eq. (13), G_0 is related to the inverse of the reservoir temperature difference squared, $(T_H-T_C)^{-2}$, which makes the cost of thermoelectric power generation sensitive to the reservoir temperature difference.

Thermoelectric power generating systems are more costly than primary power generation sources including coal, natural gas, solar, and geothermal. Primary electricity generating sources such as coal and natural gas power plants cost less than \$3/W [82], so it is unlikely that thermoelectric power generation would be considered as an alternative to these power sources, especially considering the relatively low efficiencies of thermoelectrics compared to modern Rankine and Brayton cycles. Through cost reductions, renewable energy technologies have recently become more competitive. The current cost target for photovoltaics is $\sim \$1/W$, and the photovoltaic module cost is projected to reach

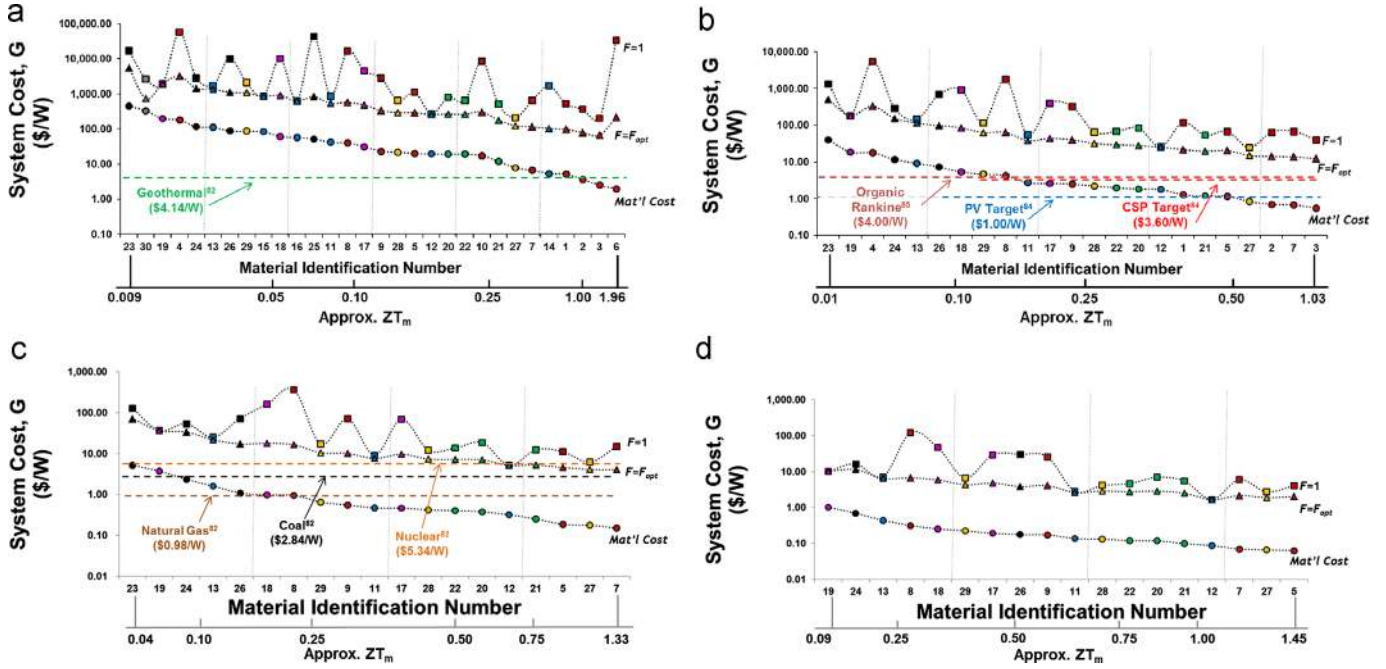


Fig. 5. Minimum cost of thermoelectric power generation, G , in $\$/W$ for materials indicated in Table 1. Comparisons are presented for the four scenarios in Table 2. Horizontal lines represent costs of competitive electricity generation technologies. The data point colors represent material class and correspond to the color legend in Figs. 6 and 7. The $F=1$ line represents a fill factor of one; the $F=F_{opt}$ line represents a module design with the optimum fill factors from Table 1. At these same $F=F_{opt}$ values, the Material' cost line ($G=4G_0F_{opt}^2$, if K_{ij} is negligible) represents the lowest obtainable cost if the heat exchanger costs and areal manufacturing costs are considered negligible. Equivalent material-only costs for other fill factors can be estimated using the Material's cost values presented here. The F_{opt} values tabulated in Table 1 can be divided out to yield $4G_0$ for each material, and another value for F can be inserted ($4G_0F^2$). Hence the material-only costs can be smaller than those plotted by more than an order of magnitude for the smallest practical F values (~ 0.01 to ~ 0.05). (a) Scenario #1: $T_H=100$ °C, $T_C=20$ °C, (b) scenario #2: $T_H=250$ °C, $T_C=20$ °C, (c) scenario #3: $T_H=500$ °C, $T_C=50$ °C and (d) scenario #4: $T_H=800$ °C, $T_C=50$ °C. (For interpretation of the references to color in this figure caption, the reader is referred to the web version of this paper.)

$\$0.50/W$ [83,84]. Although higher at $\$3\text{--}4/W$, the costs of concentrated solar power [84] and geothermal power [82] are still competitive and preferable to the costs associated with thermoelectric power generation. Key exceptions are cases where compactness and portability of the generator are critical, and many alternatives to thermoelectric power generation are not feasible due to resource availability, size, weight, and system complexity.

Thermoelectrics are especially cost competitive compared to other waste-heat recovery technologies. A competitive waste-heat recovery technology is the organic Rankine cycle (ORC) system as shown in Fig. 5b. The cost for ORC systems is approximately $\$4\text{--}5/W$ [85]. Both ORCs and thermoelectrics can be used to recover unused heat. Thermoelectrics can even be complimentary to ORCs and scavenge additional heat not recovered by the organic Rankine system [86]. The capital costs, system footprint, and maintenance costs for organic Rankine systems are considerable, so thermoelectric devices may be preferable for waste-heat recovery, particularly where reliability is paramount.

In Fig. 6, the materials can be compared considering two parameters of interest: the total areal costs of the module:

$$C''_{module} = C''L_{opt} + C'' \tag{16}$$

and the figure of merit ZT_m . The dotted reference lines are drawn for comparison to chalcogenide materials: bismuth telluride and lead telluride for low and high temperature ranges, respectively. These plots provide an image of the current materials landscape and can illustrate targets for future materials research. There is a paucity of materials in the lower right-hand quadrant which indicates new material system modules are needed that are less expensive ($C''_{module} < \$0.05/cm^2$) and higher efficiency ($ZT > 1$) than the chalcogenide reference. The clustering of points below the chalcogenide comparison material cost point indicates significant research and development work should consider material

cost while improving thermoelectric efficiency. For example, nanowire-based thermoelectric materials requiring microfabrication processes are not currently competitive options as shown in Fig. 6b and c. Materials which lie in the upper right-hand quadrant may be desirable in some instances; military applications such as mobile power sources for soldiers or space applications such as space vehicle power generators are two examples.

An important challenge is the selection of materials within a given quadrant. When faced with selecting between materials which lie in relatively close proximity to one another in Fig. 6, there are a variety of application-specific factors that govern the selection between, for example, a material having lower cost and performance and another having higher cost and performance. Such decision-making will likely rely on additional parameters related to feasibility such as material stability with respect to time, temperature, and compatibility with the operating environment, material toxicity, mechanical properties, and compatibility with metallization and other module materials, none of which are considered in this analysis.

3.3. Thermoelectric cooling

Thermoelectric cooling is an application where thermoelectrics have performed well in the market. Much of this success can be attributed to the room temperature performance of bismuth telluride alloys. However, other thermoelectric materials may also be attractive alternatives. The cost analysis discussed previously, Eq. (2) and (15), was performed on the materials listed in Table 1 and is presented in Fig. 7. Not all materials are able to achieve the targeted $\Delta T=T_1-T_2$ associated with the example application. Eq. (8) shows that if a material does not have a sufficiently large ZT for a given ΔT , then the COP is negative indicating that cooling to that ΔT cannot be achieved. The operating cost in Fig. 7 is

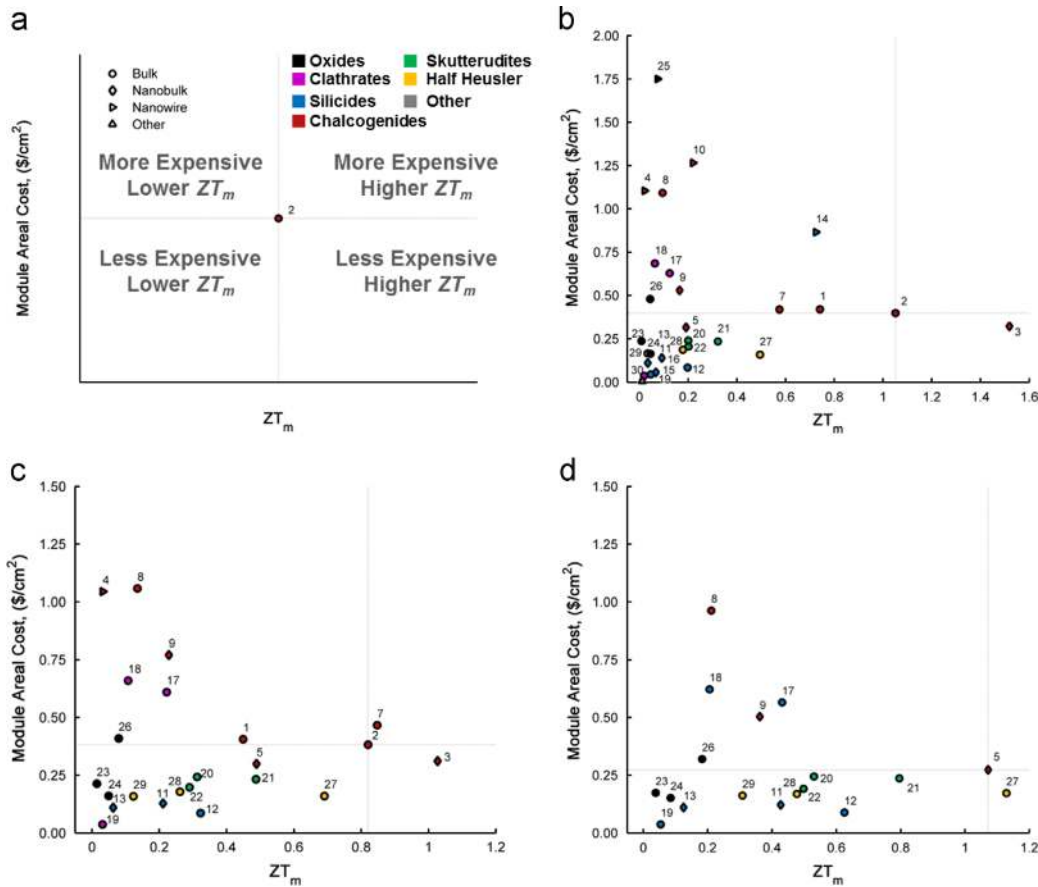


Fig. 6. Module areal cost vs. ZT_m for select thermoelectric materials with plots showing (a) the legend and (b)–(d) the various scenarios. The horizontal and vertical lines represent comparisons to reference chalcogenide materials. Materials ID# 2 and 5 from Table 1 are used for low/medium and high temperature applications, respectively. The shapes represent the manufacturing class of the material (bulk, nanobulk, nanowire, or other), and the color represents the material class. (a) Legend, (b) scenario #1: $T_H=100\text{ }^\circ\text{C}$, $T_C=20\text{ }^\circ\text{C}$, (c) scenario #2: $T_H=250\text{ }^\circ\text{C}$, $T_C=20\text{ }^\circ\text{C}$ and (d) scenario #3: $T_H=500\text{ }^\circ\text{C}$, $T_C=50\text{ }^\circ\text{C}$. (For interpretation of the references to color in this figure caption, the reader is referred to the web version of this paper.)

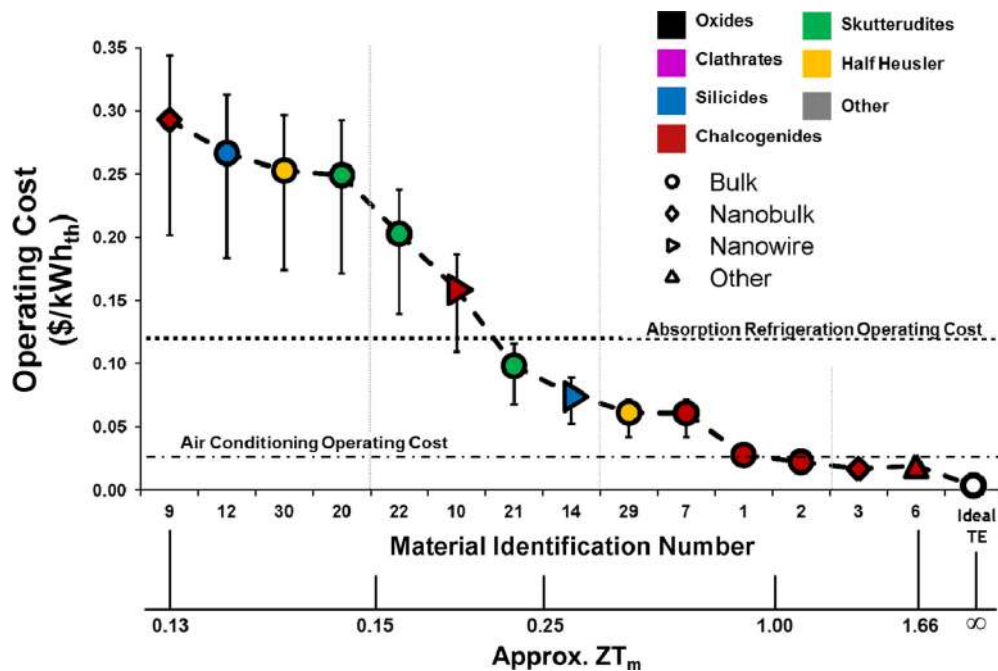


Fig. 7. Operating costs of a thermoelectric cooler for various materials and the scenario described in Table 2. Colors represent material class; shapes represent material structure resulting from different manufacturing techniques. The materials are organized from left to right in order of increasing ZT_m . The error bars represent the variability in electricity price with the average at 9.83 cents/kWh_e. The lower bound is for industrial applications with an electricity cost of 6.77 cents/kWh_e, and the upper bound is for residential applications with an electricity cost of 11.54 cents/kWh_e. In this analysis $F=1$ and the heat exchanger costs are neglected. In the ideal TE, the material is completely free and $ZT_m=\infty$; this is equivalent to a Carnot refrigerator operating with only the cost of electricity being significant, giving 0.24–0.41 cents/kWh_{th}. (For interpretation of the references to color in this figure caption, the reader is referred to the web version of this paper.)

expressed for each material at the optimum leg length that minimizes Eqs. (2) and (15) (reported in Table F.2). Materials are listed by their material identification number and are ordered by increasing ZT . There is a clear trend that larger ZT s have lower operating cost. This is because the COP is the strongest driving parameter, and the purchased electricity dominates the cost. The coefficient of performance is directly related to ZT .

The cost of thermoelectric cooling can be compared against the operating cost of absorption refrigeration and air conditioning [14,87], and many of the chalcogenides are cost competitive. Material ID #6 has the potential to be the least expensive even considering its costly MBE process. The primary challenge is making high quality superlattices with thickness approaching 130 μm , which is the optimum length as determined by this analysis. Material ID #3 also shows that the improvements in thermoelectric power output and associated cost reduction caused by nanostructuring compensate for the additional manufacturing expenses. Given the straightforward relationship to ZT , an ideal material with $ZT \approx \infty$ can have a cost of $\$0.004/\text{kW h}_{\text{th}}$ for $\Delta T = 10^\circ\text{C}$. This suggests there is still room for material improvements in cooling applications to reduce the cost even further. Cost reduction can be achieved by increasing ZT with a system capital cost that is recovered by the operating cost savings over the lifetime of the device.

3.4. Thermoelectric device targets summary

The key targets for thermoelectric devices pertain to system parameters and costs. Meeting or exceeding these targets would lead to lower cost values than those determined here. As suggested by G_0 in Eq. (13), both large ZT and small volumetric costs C''' are desirable, but they need not occur simultaneously. Materials with low ZT and low volumetric costs can have a lower $\$/W$ value than those having high ZT and high costs. Hence, there is no unique target for ZT or volumetric cost, but approximate targets can be set for current state-of-the-art system components. The heat exchanger and ceramic plate dominate the overall cost for many devices. For the situation where the heat exchanger costs dominate, improving ZT is more important than reducing C''' . The $\$1/(\text{W/K})$ target for heat exchanger cost is below the existing minimum cost [68], and U -values above $200 \text{ W/m}^2 \text{ K}$ are desirable. Ceramic plates with thermal conductivity above 40 W/m K and cost below $\$0.10/\text{cm}^2$ would reduce thermoelectric system costs. Since the areal manufacturing costs contribute minimally to the overall cost, these costs should remain at or below the current value of $\$0.01/\text{cm}^2$ for dicing and metallization of bulk materials. Any additional areal processing costs would increase this value, and gains in other parameters would need to mitigate the additional cost.

4. Conclusion

This work applies a new thermoelectrics cost analysis [34] which incorporates material properties, device physics, material costs, manufacturing costs, and system costs. The analysis and resulting cost values provide a tool for thermoelectric device research and development. Optimization of thermoelectric leg length and fill factor minimizes the ratio of cost to performance, as opposed to optimization of efficiency and power output alone. This work makes progress on evaluating the status of thermoelectric materials relative to competitive power generation technologies for a range of application temperatures. Novel nanowire and superlattice materials have the potential to have a low $\$/W$ value if improvements in ZT are made above what is reported, but with the currently reported values they are not competitive in the near-term due to the large costs associated with microfabrication/MBE manufacturing techniques. When applied to several

traditional and new thermoelectric material classes, the analysis demonstrates the paucity of materials which are both higher performing and lower cost than standard chalcogenides. However, there are multiple thermoelectric materials which could yield power generation systems that are affordable and competitive with other forms of power generation; the key challenges for these materials will be in both engineering devices around them and scaling their production. The utility of the cost metrics presented here will evolve as factors such as resource availability and energy costs change over time demonstrating the need to revisit this analysis periodically. The realization of commercial thermoelectric devices depends on the simultaneous improvement and optimization of material properties, system design, system costs, and material and manufacturing costs.

Acknowledgments

We gratefully acknowledge funding support through the NSF/DOE Partnership on Thermoelectric Devices for Vehicle Applications (Grant No. 1048796). S. LeBlanc would like to acknowledge the Sandia National Laboratories Fellowship and the Stanford DARE fellowship. S. K. Yee would like to acknowledge support from the John and Fannie Hertz Foundation and the Big George Fellowship. We would also like to thank Profs. Arun Majumdar, Gang Chen, and G. Jeffrey Snyder for their insight and discussion of this work during preparation of the manuscript.

Appendix A. Supporting information

Supplementary data associated with this article can be found in the online version at <http://dx.doi.org/10.1016/j.rser.2013.12.030>.

References

- [1] Zebarjadi M, Esfarjani K, Dresselhaus MS, Ren ZF, Chen G. Perspectives on thermoelectrics: from fundamentals to device applications. *Energy Environ Sci* 2012;5:5147.
- [2] Bell LE. Cooling, heating, generating power, and recovering waste heat with thermoelectric systems. *Science* 2008;321:1457–61.
- [3] Tritt TM. Thermoelectric phenomena, materials, and applications. *Annu Rev Mater Res* 2011;41:433–48.
- [4] Nolas GS, Poon J, Kanatzidis M. Recent developments in bulk thermoelectric materials. *MRS Bull* 2006:31.
- [5] Snyder GJ, Toberer ES. Complex thermoelectric materials. *Nat Mater* 2008;7.
- [6] Sootsman JR, Chung DY, Kanatzidis MG. New and old concepts in thermoelectric materials. *Angew Chem Int Ed Engl* 2009;48:8616–39.
- [7] Shakouri A. Recent developments in semiconductor thermoelectric physics and materials. *Annu Rev Mater Res* 2011;41:399–431.
- [8] Salvador JR, Cho JY, Ye Z, Moczygemba JE, Thompson AJ, Sharp JW, et al. Thermal to electrical energy conversion of skutterudite-based thermoelectric modules. *J Electron Mater*. <http://dx.doi.org/10.1007/s11664-012-2261-9>.
- [9] Li F, Huang X, Jiang W, Chen L. Microstructure and contact resistivity of $(\text{Bi}, \text{Sb})_2\text{Te}_3/\text{Sb}$ interface. *AIP Conf Proc* 2012;1449:458–62. <http://dx.doi.org/10.1063/1.4731595>. (28–30 September 2011, Thessaloniki, Greece).
- [10] Battistoni S, Boldrini S, Fiameni S, Famengo A, Fabrizio M, Barison S. Multilayered thin films for oxidation protection of Mg_2Si thermoelectric material at middle–high temperatures. *Thin Solid Films*, 2012;526:150–4, ISSN 0040-6090. <http://dx.doi.org/10.1016/j.tsf.2012.10.114>.
- [11] Leszczynski J, Wojciechowski K, Malecki A. Studies on thermal decomposition and oxidation of CoSb_3 . *J Therm Anal Calorim* 2011;105:211–22.
- [12] Bennet GL, Skrabek EA. Power performance of U.S. space radioisotope thermoelectric generators. In: 15th International conference on thermoelectrics; 1996.
- [13] Goodson KE, Asheghi M. Novel nanostructured interface solutions for automotive thermoelectric modules application. 3rd Department of energy thermoelectrics applications workshop. Baltimore, MD; 2012.
- [14] Goodson KE. Automotive thermoelectric modules with scalable thermo- and electro-mechanical interfaces. 2011 Thermoelectrics applications workshop. San Diego, CA: U.S. Department of Energy; 2011.
- [15] Gao Y, Marconnet AM, Panzer MA, LeBlanc S, Dogbe S, Ezzahri Y, et al. Nanostructured interfaces for thermoelectrics. *J Electron Mater* 2010;39:1456–62.

- [16] Miner A. The industrialization of thermoelectric power generation technology. 3rd Thermoelectrics applications workshop. Baltimore, MD: U.S. Department of Energy; 2012.
- [17] Yadav GG, Susoreny JA, Zhang G, Yang H, Wu Y. Nanostructure-based thermoelectric conversion: an insight into the feasibility and sustainability for large-scale deployment. *Nanoscale* 2011;3:3555–62.
- [18] Fairbanks J. Vehicular Thermoelectrics: a new green technology. Thermoelectrics Applications Workshop. San Diego, CA: Department of Energy; 2011.
- [19] Straub P. Claremont creek ventures. (personal communication).
- [20] Crane DT. Thermoelectric generator performance for passenger vehicles. 3rd Thermoelectrics applications workshop. Baltimore, MD: U.S. Department of Energy; 2012.
- [21] Aixala L. RENOTER project. 3rd Thermoelectrics applications workshop. Baltimore, MD: U.S. Department of Energy; 2012.
- [22] Crane DT, Kossakovski D. High heat flux thermoelectric module using standard bulk material. 3rd Thermoelectrics applications workshop. Baltimore, MD: U.S. Department of Energy; 2012.
- [23] Meisner G. Skutterudite thermoelectric generator for automotive waste heat recovery. 3rd Thermoelectrics applications workshop. Baltimore, MD: U.S. Department of Energy; 2012.
- [24] Karri MA, Thacher EF, Helenbrook BT. Exhaust energy conversion by thermoelectric generator: two case studies. *Energy Convers Manag* 2011;52:1596–611.
- [25] Won Y, Gao Y, Panzer MA, Dogbe S, Pan L, Kenny TW, et al. Mechanical characterization of aligned multi-walled carbon nanotube films using micro-fabricated resonators. *Carbon* 2012;50:347–55.
- [26] Gao Y, Kodama T, Won Y, Dogbe S, Pan L, Goodson KE. Impact of nanotube density and alignment on the elastic modulus near the top and base surfaces of aligned multi-walled carbon nanotube films. *Carbon* 2012.
- [27] Yazawa K, Shakouri A. Cost-efficiency trade-off and the design of thermoelectric power generators. *Environ Sci Technol* 2011;45:7548–53.
- [28] Wadia C, Albertus P, Srinivasan V. Resource constraints on the battery energy storage potential for grid and transportation applications. *J Power Sources* 2011;196:1593–8.
- [29] Wadia C, Alivisatos AP, Kammen DM. Materials availability expands the opportunity for large-scale photovoltaics deployment. *Environ Sci Technol* 2009;43:2072–7.
- [30] Angrist SW. Direct energy conversion. Boston: Allyn and Bacon, Inc.; 1965.
- [31] Rowe DM. Thermoelectrics handbook. CRC Press; 2006.
- [32] Rowe DM, Min G. Design theory of thermoelectric modules for electrical power generation. *IEE Proc – Sci Meas Technol* 1996;143:351–6.
- [33] Kristiansen NR, Snyder GJ, Nielsen HK, Rosendahl L. Waste heat recovery from a marine waste incinerator using a thermoelectric generator. *J Electron Mater* 2012;41:1024–9.
- [34] Yee SK, LeBlanc S, Goodson KE, Dames C. \$ per W metrics for thermoelectric power generation: beyond ZT. *Energy Environ Sci* 2013;6:2561–71. <http://dx.doi.org/10.1039/C3EE41504J>.
- [35] Parker WJ, Jenkins RJ. Thermal conductivity measurements on bismuth telluride in the presence of a 2 MEV Electron Beam. Orig Receipt Date: 31-DEC-611960.
- [36] Lowhorn ND, Wong-Ng W, Lu Z-Q, Martin J, Green ML, Bonevich JE, et al. Development of a Seebeck coefficient Standard Reference Material™. *J Mater Res* 2011;26:1983–92.
- [37] Xie W, Tang X, Yan Y, Zhang Q, Tritt TM. High thermoelectric performance BiSbTe alloy with unique low-dimensional structure. *J Appl Phys* 2009;105:113713.
- [38] Zhou J, Jin C, Seol JH, Li X, Shi L. Thermoelectric properties of individual electrodeposited bismuth telluride nanowires. *Appl Phys Lett* 2005;87:133109.
- [39] Andrews SC, Fardy MA, Moore MC, Aloni S, Zhang M, Radmilovic V, et al. Atomic-level control of the thermoelectric properties in polytypoid nanowires. *Chem Sci* 2011;2:706.
- [40] Harman TC, Taylor PJ, Walsh MP, LaForge BE. Quantum dot superlattice thermoelectric materials and devices. *Science* 2002;297:2229–32.
- [41] Hsu KF, Loo S, Guo F, Chen W, Dyck JS, Uher C, et al. Cubic AgPb₁₃SbTe_{2+m}: bulk thermoelectric materials with high figure of merit. *Science* 2004;303:818–21.
- [42] Joshi G, Lee H, Lan Y, Wang X, Zhu G, Wang D, et al. Enhanced thermoelectric figure-of-merit in nanostructured p-type silicon germanium bulk alloys. *Nanoletters* 2008;8:4670–4.
- [43] Martinez JA, Provencio PP, Picraus ST, Sullivan JP, Swartzentruber BS. Enhanced thermoelectric figure of merit in SiGe alloy nanowires by boundary and hole-phonon scattering. *J Appl Phys* 2011;110:074317.
- [44] Bux SK, Yeung MT, Toberer ES, Snyder GJ, Kaner RB, Fleurial J-P. Mechanochemical synthesis and thermoelectric properties of high quality magnesium silicide. *J Mater Chem* 2011;21:12259.
- [45] Zaitsev VK, Fedorov MI, Gurieva EA, Eremin IS, Konstantinov PP, Samunin AY, et al. Highly effective Mg₂Si_{1-x}N_x thermoelectrics. *Phys Rev B* 2006;74:045207.
- [46] Bux SK, Blair RG, Gogna PK, Lee H, Chen G, Dresselhaus MS, et al. Nanostructured bulk silicon as an effective thermoelectric material. *Adv Funct Mater* 2009;19:2445–52.
- [47] Hochbaum AI, Chen R, Delgado RD, Liang W, Garnett EC, Najarian M, et al. Enhanced thermoelectric performance of rough silicon nanowires. *Nature* 2008;451:163–7.
- [48] Chen X, Weathers A, Moore A, Zhou J, Shi L. Thermoelectric properties of cold-pressed higher manganese silicides for waste heat recovery. *J Electron Mater* 2012;41:1564–72.
- [49] Cederkrantz D, Nygren M, Palmqvist AEC. Thermoelectric properties of partly Sb- and Zn-substituted Ba₈Ga₁₆Ge₃₀ clathrates. *J Appl Phys* 2010;108:113711.
- [50] Toberer E, Christensen M, Iversen B, Snyder G. High temperature thermoelectric efficiency in Ba₈Ga₁₆Ge₃₀. *Phys Rev B* 2008;77.
- [51] Roudebush JH, Toberer ES, Hope H, Jeffrey Snyder G, Kauzlarich SM. Crystal structure, characterization and thermoelectric properties of the type-I clathrate Ba₈-ySryAl₁₄Si₃₂ (0.6 ≤ y ≤ 1.3) prepared by aluminum flux. *J Solid State Chem* 2011;184:1176–85.
- [52] Qiu PF, Yang J, Liu RH, Shi X, Huang XY, Snyder GJ, et al. High-temperature electrical and thermal transport properties of fully filled skutterudites RFe₄Sb₁₂ (R=Ca, Sr, Ba, La, Ce, Pr, Nd, Eu, and Yb). *J Appl Phys* 2011;109:063713.
- [53] Peng J, He J, Alboni PN, Tritt TM. Synthesis and thermoelectric properties of the double-filled skutterudite Yb_{0.2}In_yCo₄Sb₁₂. *J Electron Mater* 2009;38:981–4.
- [54] Puyet M, Dauscher A, Lenoir B, Dehmas M, Stiewe C, Muller E, et al. Beneficial effect of Ni substitution on the thermoelectric properties in partially filled Ca_yCo_{4-x}Ni_xSb₁₂ skutterudites. *J Appl Phys* 2005;97:083712.
- [55] Tsubota T, Ohtaki M, Eguchi K, Arai H. Thermoelectric properties of Al-doped ZnO as a promising oxide material for high-temperature thermoelectric conversion. *J Mater Chem* 1997;7:85–90.
- [56] Xu G, Funahashi R, Shikano M, Matsubara I, Zhou Y. Thermoelectric properties of the Bi- and Na-substituted Ca₃Co₄O₉ system. *Appl Phys Lett* 2002;80:3760.
- [57] Fujita K, Mochida T, Nakamura K. High-temperature thermoelectric properties of Na_xCoO₂ single crystals. In: International conference on thermoelectrics; 2001. p. 168–71.
- [58] Sakurada S, Shutoh N. Effect of Ti substitution on the thermoelectric properties of (Zr,Hf)NiSn half-Heusler compounds. *Appl Phys Lett* 2005;86:082105.
- [59] Shen Q, Chen L, Goto T, Hirai T, Yang J, Meisner GP, et al. Effects of partial substitution of Ni by Pd on the thermoelectric properties of ZrNiSn-based half-Heusler compounds. *Appl Phys Lett* 2001;79:4165.
- [60] Katayama T, Kim S, Kimura Y, Mishima Y. The effects of quaternary additions on thermoelectric properties of TiNiSn-based half-Heusler alloys. *J Electron Mater* 2003;32:1160–5.
- [61] Scholdt M, Do H, Lang J, Gall A, Colsmann A, Lemmer U, et al. Organic semiconductors for thermoelectric applications. *J Electron Mater*.2010;39:1589–1592. <http://dx.doi.org/10.1007/s11664-010-1271-8>.
- [62] Kraemer D, Poudel B, Feng H-P, Caylor JC, Yu B, Yan X, et al. High-performance flat-panel solar thermoelectric generators with high thermal concentration. *Nat Mater* 2011 (advance online publication).
- [63] Imry Y, Landauer R. Conductance viewed as transmission. *Rev Mod Phys* 1999;71:S306–12.
- [64] Min G, Rowe DM. Conversion efficiency of thermoelectric combustion systems. *IEEE Trans Energy Convers* 2007;22.
- [65] Rowe MD, Min G, Williams SGK, Aoune A, Matsuura K, Kuznetsov VL, et al. Thermoelectric recovery of waste heat – case studies. In: 32nd intersociety energy conversion engineering conference; 1997.
- [66] Snyder G, Ursell T. Thermoelectric efficiency and compatibility. *Phys Rev Lett* 2003;91.
- [67] Yazawa K, Shakouri A. Optimization of power and efficiency of thermoelectric devices with asymmetric thermal contacts. *J Appl Phys* 2012;111:024509.
- [68] Shah RK, Sekuli P.Da. Fundamentals of heat exchanger design. John Wiley & Sons.
- [69] Mayer PM, Ram RJ. Optimization of heat sink-limited thermoelectric generators. *Nanoscale Microscale Thermophys* 2006;10:143–55.
- [70] Branker K, Pathak MJM, Pearce JM. A review of solar photovoltaic leveled cost of electricity. *Renew Sustain Energy Rev* 2011;15:4470–82.
- [71] Matthews LM. Estimating manufacturing costs: a practical guide for managers and estimators. New York: McGraw-Hill; 1983.
- [72] U.S. Geological Survey: Commodity Statistics Information. U.S. Department of Interior; 2011.
- [73] Wu C-I, Girard SN, Sootsman J, Timm E, Case ED, Kanatzidis MG, et al. Novel lead telluride based thermoelectric materials. *MRS Proc* 2011:1314.
- [74] Tom Carver Science & Engineering Associate. Science & Engineering Associate, Flexible Cleanroom and Microfab Shop, Stanford Nano Center; 2012. (personal communication).
- [75] Niu X, Yu J, Wang S. Experimental study on low-temperature waste heat thermoelectric generator. *J Power Sources* 2009;188:621–6.
- [76] Hansen RC. Overall equipment effectiveness: a powerful production/maintenance tool for increased profits. 1st ed.. New York: Industrial Press Inc.; 2002.
- [77] Beekman M, Nolas GS. Inorganic clathrate-II materials of group 14: synthetic routes and physical properties. *J Mater Chem* 2008;18:842.
- [78] LaLonde AD, Pei Y, Wang H, Jeffrey Snyder G. Lead telluride alloy thermoelectrics. *Mater Today* 2011;14:526–32.
- [79] Disco (www.disco.co.jp).
- [80] Biswas K, He J, Blum ID, Wu C-I, Hogan TP, Seidman DN, et al. High-performance bulk thermoelectrics with all-scale hierarchical architectures. *Nature* 2012;489:414–8.
- [81] Vining CB. An inconvenient truth about thermoelectrics. *Nat Mater* 2009;8:83–5.
- [82] Koumoto K, Wang Y, Zhang R, Kosuga A, Funahashi R. Oxide thermoelectric materials: a nanostructuring approach. *Annu Rev Mater Res* 2010;40:363–94.
- [83] Powell DM, Winkler MT, Choi HJ, Simmons CB, Needleman DB, Buonassisi T. Crystalline silicon photovoltaics: a cost analysis framework for determining

- technology pathways to reach baseload electricity costs. *Energy Environ Sci* 2012;5:5874.
- [84] US Department of Energy, Sunshot vision study; 2012.
- [85] Vélez F, Segovia JJ, Martín MC, Antolín G, Chejne F, Quijano A. A technical, economical and market review of organic Rankine cycles for the conversion of low-grade heat for power generation. *Renew Sustain Energy Rev* 2012;16:4175–89.
- [86] Miller E, Hendricks T, Peterson R. Modeling energy recovery using thermoelectric conversion integrated with an organic rankine bottoming cycle. *J Electron Mater* 2009;38:1206–13.
- [87] Esarte J, Min G, Rowe DM. Modelling heat exchangers for thermoelectric generators. *J Power Sources* 2001:93.